Received 3 October 2017; revised 20 November 2017; accepted 4 December 2017. Date of publication 8 December 2017; date of current version 15 January 2018. The review of this paper was arranged by Editor S. Vaziri.

Digital Object Identifier 10.1109/JEDS.2017.2781250

Contact Resistance Reduction of WS_2 FETs Using High-Pressure Hydrogen Annealing

YUN JI KIM, WOOJIN PARK, JIN HO YANG, YONGHUN KIM, AND BYOUNG HUN LEE, (Senior Member, IEEE)

Center for Emerging Electronic Devices and Systems, School of Material Science and Engineering, Gwangju Institute of Science and Technology, Gwangju 61005, South Korea

CORRESPONDING AUTHOR: B. H. LEE (e-mail: bhl@gist.ac.kr)

This work was supported in part by the Global Frontier Research and Development Program at the Center for Hybrid Interface Materials through the National Research Foundation of Korea funded by the Ministry of Science and ICT under Grant 2013M3A6B1078873, and in part by the Nano-Material Technology Development Program through the National Research foundation of Korea (NRF) funded by the Ministry of Science, ICT and Future Planning under Grant 2016M3A7B4909942. *(Yun Ji Kim and Woojin Park contributed equally to this work.)*

ABSTRACT The transition metal dichalcogenides (TMDCs) have been extensively investigated for various applications such as logic, memory and optical devices, and sensors. The pressing challenge in the research of TMDCs is the electrical performance limited by the high contact resistance. We report more than 5000 times reduction in the contact resistance of WS_2 field-effect transistor (FET) with Ti contact (81 MΩ μm to 14.6 kΩ μm) by high-pressure hydrogen annealing. Schottky barrier height reduction appears to play a major role in the reduction of the contact resistance. This process can be used to reduce the contact resistance even further by combining with a doping technique for TMDCs and a contact metal optimization for TMDC FETs.

INDEX TERMS Contact resistance, Fermi-level depinning, high-pressure hydrogen annealing, WS_2 FET.

I. INTRODUCTION

Recently, transition metal dichalcogenides (TMDCs) have generated significant research interest due to its unique electrical, optical, and mechanical properties [1]–[5]. Their applications in various devices such as field-effect transistors (FETs), memory devices, optical devices, and multifunctional sensors have been actively investigated [6]–[15]. For example, Radisavljevic *et al.* [6] demonstrated a single-layer MoS_2 FET for the first time, with high field effect mobility (μ_{FE}) of over 200 cm^2/Vs. Bertolazzi *et al.* [10] demonstrated a MoS_2 non-volatile memory cell with a graphene floating layer. TMDCs have unique advantages in thin film transistor (TFT) applications, because of relatively high μ_{FE} (30–100 cm^2/Vs) compared to other materials such as organic TFT or a-Si TFT [13], [14].

In spite of the promising initial results, several technical challenges need to be overcome in order to consider TMDCs for practical electronics and display applications. Thus, a significant number of studies have been actively conducted on the various aspects of the integration processes that affect gate dielectric, contact resistance, interface, and reliability, to improve the performance of TMDC FETs. The performance of single layer MoS_2 FETs could be substantially improved with a high-k gate dielectric, which reduced the carrier scattering ($\mu_{FE} \sim 200$ cm^2/Vs) [6]. Several approaches to reduce the contact resistance of TMDC FETs have been reported, including molecule or Cl doping techniques, the use of low work function contact metal, and the use of Fermi-level depinning layer [16]–[20]. In particular, the method of Fermi-level depinning using a thin interlayer dielectric is found to be effective in the reduction of low-frequency noise in multilayer MoS_2 FETs [21]. Dielectric passivation techniques have also been investigated to improve the stability of TMDC FETs [22], [23].

In this study, we analyzed the effect of high-pressure hydrogen annealing (HPHA) on the performance of WS_2 FETs in terms of drive current, conduction mechanism and contact resistance. The mechanism of the three-fold increase in the drive current and the conduction mechanism change from bipolar to close-to-unipolar have been identified.

II. EXPERIMENT

WS_2 (HQ graphene) flakes were transferred onto SiO_2 (90 nm)/silicon substrates by a mechanical

2168-6734 © 2017 IEEE. Translations and content mining are permitted for academic research only.
Personal use is also permitted, but republication/redistribution requires IEEE permission.
See http://www.ieee.org/publications_standards/publications/rights/index.html for more information.

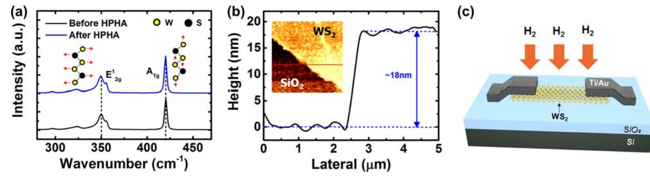

FIGURE 1. (a) Raman spectra for multi-layer WS_2 before and after the HPHA. (b) The thickness of multi-layer WS_2 measured by AFM and the inset figure shows the image of WS_2. (c) Schematic of WS_2 FET with HPHA (20 atm, 300 °C, 30 min).

exfoliation process. The optical characteristics of the transferred bilayer and multilayer WS_2 were evaluated using Raman spectroscopy (RENISHAW in ViaRaman microscope, laser wavelength: 514 nm, 50 mW). Fig. 1(a) shows representative Raman spectra of a multilayer WS_2 before and after the HPHA. The thickness of WS_2 flakes can be roughly estimated from the frequency difference between E^1_{2g} (in-plane vibrational motion) and A_{1g}(out-of-plane vibrational motion). As the thickness of WS_2 increases, the E^1_{2g} mode shows redshifts, while the A_{1g} mode shows blueshifts [24], [25]. Fig. 1(b) shows the thickness of the multilayer WS_2 flake measured by non-contact atomic force microscopy (AFM) and the inset shows the AFM image of the multilayer WS_2. The thickness of the multilayer WS_2 was approximately 18 nm. The schematic of WS_2 FET is shown in Fig. 1(c). After transferring WS_2 onto SiO_2, the source and drain electrodes (Ti/Au) were deposited using e-beam evaporation and patterned using a lift-off process. The channel length and width were 3 μm and 6 μm, respectively. Finally, the HPHA was performed at 20 atm and 300 °C for 30 min. The process condition of HPHA used in this work was determined to maximize the introduction of hydrogen and minimize the damage to the WS_2 layer [26], [27]. The Raman spectra of WS_2 before and after the HPHA shown in Fig. 1(a) indicate that there is no noticeable change in the quality of WS_2 after the HPHA.

III. RESULT AND DISCUSSION

Fig. 2(a) shows the transfer characteristics (I_{DS}–V_{BG}) of the WS_2 FET before and after the HPHA. Before the HPHA, the electron current was relatively low, indicating a significantly high channel resistance and bipolar type *I-V* characteristics involving both electron and hole currents were observed as previously reported in [16] and [28]. On the other hand, the *I-V* characteristics were substantially changed after the HPHA. The transfer curve and threshold voltage (V_{TH}) was shifted to the negative direction after the HPHA [29]. Since TMDC FETs are basically Schottky junction FETs, SBH reduction with contact engineering tends to reduce the threshold voltage. Average drain current increased by ~3 times from 0.127 μA/μm to 0.32 μA/μm after the HPHA. The off current was slightly increased after the HPHA, but the difference was small.

The enhancement in the electron current was also confirmed in the output characteristics ($I_{DS} - V_{DS}$) also (Fig. 2(c) and (d)). The shape of output current curve provides the clue

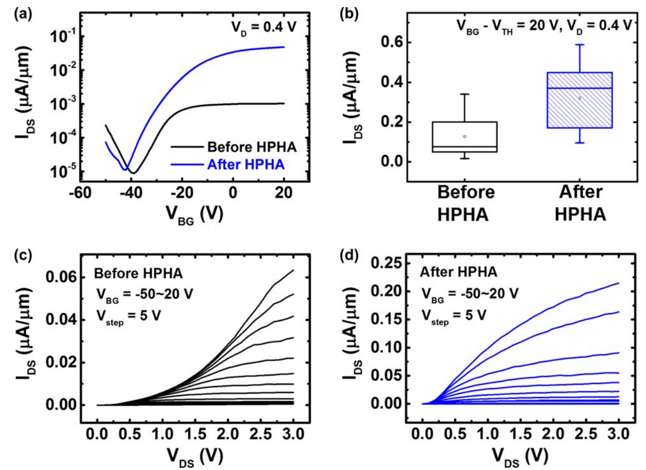

FIGURE 2. (a) I_{DS}-V_{BG} of WS_2 FET before/after the HPHA. (b) The average width normalized drain current before/after the HPHA at V_{BG}-V_{TH} = 20 V. I_{DS}-V_{DS} curves of WS_2 FET (c) before and (d) after the HPHA.

to the origin of performance enhancement. The envelope curve of Fig. 2(c) follows the path of a quadratic curve, which indicates the presence of a high series resistance. After the HPHA, the output curves shown in Fig. 2(d) exhibited quadratic saturation characteristics and the drain current increased by more than 300%. This enhancement could be explained by the interface state passivation by the hydrogen as in the case of silicon and a reduction in the contact resistance. In either case, more detailed analysis is necessary to understand the actual mechanism of improvement.

First, we investigated the change in the interface states of WS_2 channel after the HPHA. Unfortunately, in case of WS_2 FETs, charge pumping method could not be used due to the high series resistance. Therefore, a relatively rough comparison was performed using the subthreshold slope (*SS*) from $I_{DS} - V_{BG}$ of WS_2 FET using the following equation [30].

$$SS = \frac{dV_g}{d\left(\log_{10} I_d\right)} = \ln 10 \cdot \frac{kT}{q}\left(1 + \frac{C_s + C_{it}}{C_{ox}}\right) \approx 60mV\left(1 + \frac{C_{it}}{C_{ox}}\right) \quad (1)$$

where C_{it} is the capacitance related to the interface trap density ($C_{it} = qD_{it}$), C_{ox} is the oxide capacitance which is $38.35 nF/cm^2$ in this work. The average interface trap densities of the WS_2 FETs decreased from 3.39×10^{13} $eV^{-1}cm^{-2}$ to 1.73×10^{13} $eV^{-1}cm^{-2}$ after the HPHA as shown in Fig. 3(a). Even though the density of interface states decreased by about 49%, this change was not enough to explain 300% enhancement in the drive current.

Next, the influence of HPHA on the contact resistance was investigated. The series resistance between the source and drain (R_{SD}), including the contact resistance, was obtained from the ratio between two $I_{DS} - V_{BG}$ curves measured at different drain biases [16], [31]. The R_{SD} could be extracted with an assumption that the contact resistance is not affected by the drain bias. Fig. 3(b) shows the total resistance

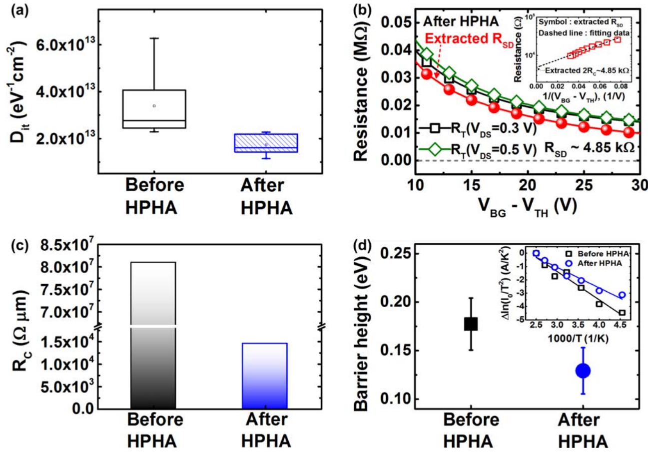

FIGURE 3. **(a) D_{it} for the eight devices and (b) R_T for V_{DS} = 0.3 V and 0.5 V including the extracted R_{SD} for WS_2 FET after HPHA. Inset figure shows the extracted $2R_C$ at the high gate overdrive ($1/(V_{BG} - V_{TH}) \sim 0V^{-1}$). (c) Comparison of extracted R_C before/after the HPHA. (d) SBH with Ti contact and the inset figure shows the Arrhenius plots for before/after the HPHA.**

($R_T = V_{DS}/I_{DS}$) as a function of gate overdrive for the two drain biases (V_{DS} = 0.3 and 0.5 V) and the R_{SD} for the WS_2 FET after the HPHA. Since R_T of WS_2 FET is the sum of the channel resistance and series resistance ($R_T = R_{SD} + R_{Channel}$), the R_{SD} can be extracted using two different channel resistance values at a high overdrive bias. The detail explanation of the method used to calculate the series resistance can be found in [21]. The inset figure in Fig. 3(b) shows the extrapolation curve to extract the contact resistance at a high gate-overdrive condition ($1/(V_{BG}-V_{TH}) \sim 0$ V^{-1}) by fitting the $R_{SD} - 1/(V_{BG} - V_{TH})$ curve.

The extrapolated R_{SD} values were approximately 27 MΩ before and 4.85 kΩ after the HPHA. The contact resistance, R_C, which is roughly equal to the half of R_{SD}, decreased by more than 5000 times. Fig. 3(c) shows the length normalized contact resistance, R_C of the WS_2 FET. After the HPHA, the R_C was drastically decreased to 14.55 kΩμm from 81 MΩμm. This result is very encouraging because more than three orders of magnitude reductions in the contact resistance was achieved without any additional doping or depinning layer, even though the final value of R_C is still slightly higher than the previously reported results in the literature (Table 1). However, once the mechanism of the improvement is fully understood, there is a possibility to use the HPHA in combination with the methods listed in Table 1 to reduce the R_C further.

Then, the SBH at the metal and WS_2 contact were analyzed using the temperature dependence of the drive current to investigate the influence of HPHA. The barrier height was extracted using the Richardson-Schottky equation shown below [16], [31].

$$I = AA^*T^2 \exp\left[-\frac{\left(\phi_B - \sqrt{q^3V/4\pi\varepsilon_0\varepsilon_r d}\right)}{k_B T}\right] \quad (2)$$

TABLE 1. **R_C And μ_{FE} for WS_2 FETs With Various Treatments.**

	Contact metal	Methods	R_C [kΩ μm]	μ_{FE} [$cm^2V^{-1}s^{-1}$]
This work	Ti	HPHA	14.55	13
[16]	Ti	Dielectric layer	24	19
[17]	Ni	Cl doping	0.7	60
[18]	Graphene	1D graphene contact	20	14
[19]	Cr	KI doping	3.75	255
[20]	Cr	LiF	0.9	34.7

where A is the contact area, A^* is the effective Richardson constant, ϕ_B is the SBH, q is the electron charge, V is the applied forward bias, ε_0 and ε_r are the permittivity of vacuum and WS_2 respectively, d is the width of the interface barrier, k_B is the Boltzmann constant, and T is the temperature. The inset of Fig. 3(d) shows the Arrhenius plot for the WS_2 FET before and after the HPHA. For the barrier height extraction, I_{DS}-V_{DS} was measured at the temperature range from 200 K to 400 K, and I_0 value was extracted at $V_{DS} = 0$ V. The SBH was calculated from the slope of Arrhenius plot ($\ln(I_0/T^2) - 1/T$). The average SBH is found to be reduced from 0.18 eV to 0.13 eV after the HPHA. The difference ~50 meV in the SBH seems to be small to explain the change in the drive current. Interestingly, drastically enhanced device performance in TMDC FETs with relatively small change in SBH was also reported by other groups. Das *et al.* [7] reported that ~5 times increased drain current was achieved with high mobility by reducing only 20 meV of Schottky barrier [7]. Thus, there is a possibility that the SBH measurement method might not be accurate for TMDC FETs, or there might be additional factors affecting the performance of TMDC FETs other than D_{it} and R_c.

Then, how the HPHA would have affected the SBH? Fermi-level pinning effects at the metal contact of multilayer and monolayer TMDCs materials have been reported in [7] and [32]. The SBH at the interface of Ti and multilayer TMDCs was found to be higher than the theoretical prediction [19]. The previous study on the hydrogenation of MoS_2 might provide the clue [33]. If the hydrogenation reaction happened at the interface of Ti and WS_2 reduced the SBH, it may result in the Fermi-level depinning like behaviors. Also, the recent study on the effect of HPHA on metal and graphene also indicates that the hydrogen can penetrate into the interface of metal and TMDC materials [27].

This hypothesis can explain the change in the current conduction mechanism also. As the SBH decreased after the HPHA, the electron conduction could become dominant while the hole current was suppressed as schematically illustrated in Fig. 4, resulting in the close-to-unipolar conduction behavior. Even though the details role of hydrogen at the interface of metal and WS_2 will require more theoretical studies, the experimental evidence such as the drastic

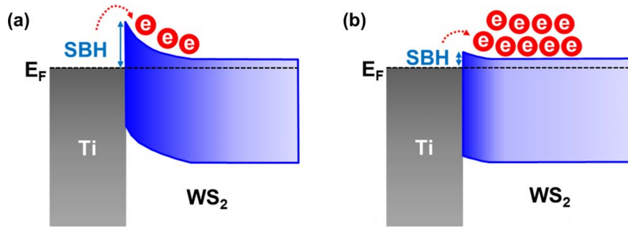

FIGURE 4. Band diagram of metal (Ti) and WS_2 contact (a) before and (b) after the HPHA. The band diagram after the HPHA illustrates that the electron current is enhanced by the SBH decrease.

R_C reduction, SBH reduction, and conduction mechanism change point that the Fermi-level alignment was changed after the HPHA, i.e., Fermi-level depinning effect.

We have not explored another possibility such as the bulk defects of WS_2 which might have been passivated by hydrogen and improved the performance of FETs. At this point, the quality of WS_2 channel was not sufficient to separately identify the contributions of the interface state and bulk defects.

IV. CONCLUSION

HPHA has been identified as an effective method to reduce the R_C of WS_2 FETs. Three orders of magnitude reduction at the R_C were attributed to the reduction of SBH via the hydrogen related reaction at the interface of Ti and WS_2. Even though the final R_C is still higher than other approaches, HPHA has an advantage that it can be easily combined with other approaches to reduce the R_C such as doping or low work function metal, because it can be performed after the device fabrication.

REFERENCES

[1] M. Palummo, M. Bernardi, and J. C. Grossman, "Exciton radiative lifetimes in two-dimensional transition metal dichalcogenides," *Nano Lett.*, vol. 15, no. 5, pp. 2794–2800, Mar. 2015, doi: 10.1021/nl503799t.

[2] H. Li *et al.*, "Optical identification of single- and few-layer MoS_2 sheets," *Small*, vol. 8, no. 5, pp. 682–686, Jan. 2012, doi: 10.1002/smll.201101958.

[3] S. Bertolazzi, J. Brivio, and A. Kis, "Stretching and breaking of ultrathin MoS_2," *ACS Nano*, vol. 5, no. 12, pp. 9703–9709, Nov. 2011, doi: 10.1021/nn203879f.

[4] A. Castellanos-Gomez *et al.*, "Elastic properties of freely suspended MoS_2 nanosheets," *Adv. Mater.*, vol. 24, no. 6, pp. 772–775, Feb. 2012, doi: 10.1002/adma.201103965.

[5] G. A. Salvatore *et al.*, "Fabrication and transfer of flexible few-layers MoS_2 thin film transistors to any arbitrary substrate," *ACS Nano*, vol. 7, no. 10, pp. 8809–8815, Aug. 2013, doi: 10.1021/nn403248y.

[6] B. Radisavljevic, A. Radenovic, J. Brivio, V. Giacometti, and A. Kis, "Single-layer MoS_2 transistors," *Nat Nano*, vol. 6, no. 3, pp. 147–150, Jan. 2011, doi: 10.1038/nnano.2010.279.

[7] S. Das, H.-Y. Chen, A. V. Penumatcha, and J. Appenzeller, "High performance multilayer MoS_2 transistors with scandium contacts," *Nano Lett.*, vol. 13, no. 1, pp. 100–105, Dec. 2012, doi: 10.1021/nl303583v.

[8] B. Radisavljevic, M. B. Whitwick, and A. Kis, "Integrated circuits and logic operations based on single-layer MoS_2," *ACS Nano*, vol. 5, no. 12, pp. 9934–9938, Nov. 2011, doi: 10.1021/nn203715c.

[9] H. Wang *et al.*, "Integrated circuits based on bilayer MoS_2 transistors," *Nano Lett.*, vol. 12, no. 9, pp. 4674–4680, Aug. 2012, doi: 10.1021/nl302015v.

[10] S. Bertolazzi, D. Krasnozhon, and A. Kis, "Nonvolatile memory cells based on MoS_2/graphene heterostructures," *ACS Nano*, vol. 7, no. 4, pp. 3246–3252, Mar. 2013, doi: 10.1021/nn3059136.

[11] H. S. Lee *et al.*, "MoS_2 nanosheets for top-gate nonvolatile memory transistor channel," *Small*, vol. 8, no. 20, pp. 3111–3115, Oct. 2012, doi: 10.1002/smll.201200752.

[12] S. Wi *et al.*, "Enhancement of photovoltaic response in multilayer MoS_2 induced by plasma doping," *ACS Nano*, vol. 8, no. 5, pp. 5270–5281, May. 2014, doi: 10.1021/nn5013429.

[13] S. Jo, N. Ubrig, H. Berger, A. B. Kuzmenko, and A. F. Morpurgo, "Mono- and bilayer WS_2 light-emitting transistors," *Nano Lett.*, vol. 14, no. 4, pp. 2019–2025, Mar. 2014, doi: 10.1021/nl500171v.

[14] J. Kwon *et al.*, "Optically transparent thin-film transistors based on 2D multilayer MoS_2 and indium zinc oxide electrodes," *Nanotechnology*, vol. 26, no. 3, Jan. 2015, Art. no. 035202, doi: 10.1088/0957-4484/26/3/035202.

[15] Z. Yin *et al.*, "Single-layer MoS_2 phototransistors," *ACS Nano*, vol. 6, no. 1, pp. 74–80, Jan. 2012, doi: 10.1021/nn2024557.

[16] W. Park *et al.*, "Complementary unipolar WS_2 field-effect transistors using Fermi-level depinning layers," *Adv. Electron. Mater.*, vol. 2, no. 2, Feb. 2016, Art. no. 1500278, doi: 10.1002/aelm.201500278.

[17] L. Yang *et al.*, "Chloride molecular doping technique on 2D materials: WS_2 and MoS_2," *Nano Lett.*, vol. 14, no. 11, pp. 6275–6280, Oct. 2014, doi: 10.1021/nl502603d.

[18] M. H. D. Guimarães *et al.*, "Atomically thin ohmic edge contacts between two-dimensional materials," *ACS Nano*, vol. 10, no. 6, pp. 6392–6399, Jun. 2016, doi: 10.1021/acsnano.6b02879.

[19] M. W. Iqbal *et al.*, "Tailoring the electrical and photo-electrical properties of a WS_2 field effect transistor by selective n-type chemical doping," *RSC Adv.*, vol. 6, no. 29, pp. 24675–24682, Mar. 2016, doi: 10.1039/C6RA02390H.

[20] H. M. W. Khalil, M. F. Khan, J. Eom, and H. Noh, "Highly stable and tunable chemical doping of multilayer WS_2 field effect transistor: Reduction in contact resistance," *ACS Appl. Mater. Interfaces*, vol. 7, no. 42, pp. 23589–23596, Oct. 2015, doi: 10.1021/acsami.5b06825.

[21] Y. Kim *et al.*, "Reduction of low-frequency noise in multilayer MoS_2 FETs using a Fermi-level depinning layer," *Physica Status Solidi Rapid Res. Lett.*, vol. 10, no. 8, pp. 634–638, Aug. 2016, doi: 10.1002/pssr.201600136.

[22] D. Jena and A. Konar, "Enhancement of carrier mobility in semiconductor nanostructures by dielectric engineering," *Phys. Rev. Lett.*, vol. 98, no. 13, Mar. 2007, Art. no. 136805, doi: 10.1103/PhysRevLett.98.136805.

[23] C.-K. Kim *et al.*, "Highly stable 2D material (2DM) field-effect transistors (FETs) with wafer-scale multidyad encapsulation," *Nanotechnology*, vol. 28, no. 5, Dec. 2016, Art. no. 055203, doi: 10.1088/1361-6528/aa5235.

[24] A. Berkdemir *et al.*, "Identification of individual and few layers of WS_2 using Raman spectroscopy," *Sci. Rep.*, vol. 3, p. 1755, Apr. 2013, doi: 10.1038/srep01755.

[25] W. Park *et al.*, "Characteristics of a pressure sensitive touch sensor using a piezoelectric PVDF-TrFE/MoS_2 stack," *Nanotechnology*, vol. 24, no. 47, Oct. 2013, Art. no. 475501, doi: 10.1088/0957-4484/24/47/475501.

[26] G. Ye *et al.*, "Defects engineered monolayer MoS_2 for improved hydrogen evolution reaction," *Nano Lett.*, vol. 16, no. 2, pp. 1097–1103, Feb. 2016, doi: 10.1021/acs.nanolett.5b04331.

[27] Y. J. Kim *et al.*, "Demonstration of complementary ternary graphene field-effect transistors," *Sci. Rep.*, vol. 6, Dec. 2016, Art. no. 39353, doi: 10.1038/srep39353.

[28] W. S. Hwang *et al.*, "Transistors with chemically synthesized layered semiconductor WS_2 exhibiting 10^5 room temperature modulation and ambipolar behavior," *Appl. Phys. Lett.*, vol. 101, no. 1, Jul. 2012, Art. no. 013107, doi: 10.1063/1.4732522.

[29] C. D. English, G. Shine, V. E. Dorgan, K. C. Saraswat, and E. Pop, "Improved contacts to MoS_2 transistors by ultra-high vacuum metal deposition," *Nano Lett.*, vol. 16, no. 6, pp. 3824–3830, Jun. 2016, doi: 10.1021/acs.nanolett.6b01309.

[30] S. Kim *et al.*, "High-mobility and low-power thin-film transistors based on multilayer MoS_2 crystals," *Nat. Commun.*, vol. 3, p. 1011, Aug. 2012, doi: 10.1038/ncomms2018.

[31] W. Park *et al.*, "Contact resistance reduction using Fermi level depinning layer for MoS_2 FETs," in *Proc. IEEE Int. Electron Devices Meeting*, San Francisco, CA, USA, Dec. 2014, pp. 5.1.1–5.1.4, doi: 10.1109/IEDM.2014.7046986.
[32] C. Kim *et al.*, "Fermi level pinning at electrical metal contacts of monolayer molybdenum dichalcogenides," *ACS Nano*, vol. 11, no. 2, pp. 1588–1596, Jan. 2017, doi: 10.1021/acsnano.6b07159.
[33] S. W. Han *et al.*, "Hydrogenation-induced atomic stripes on the 2H-MoS_2 surface," *Phys. Rev. B, Condens. Matter*, vol. 92, no. 24, Dec. 2015, Art. no. 241303, doi: 10.1103/PhysRevB.92.241303.

YUN JI KIM is currently pursuing the Integrated M.S. and Ph.D. degrees in material science and engineering with the Gwangju Institute of Science and Technology, Gwangju, South Korea.

WOOJIN PARK received the Ph.D. degree in material science and engineering from the Gwangju Institute of Science and Technology, Gwangju, South Korea, in 2016.

His current research interests are 2-D material-based various functional devices.

JIN HO YANG received the M.S. and Ph.D. degrees in material science and engineering from the Gwangju Institute of Science and Technology, Gwangju, South Korea, in 2005 and 2017, respectively.

JONGHUN KIM received the Ph.D. degree in materials science and engineering from the Gwangju Institute of Science and Technology, Gwangju, South Korea, in 2016. He is a Senior Research Scientist with the Korea Institute of Materials Science.

His current research includes the synthesis of emerging 2-D nanomaterials, semiconductor integrated process, neuromorphic synapse electronic materials and devices, and advanced electrical characterization.

BYOUNG HUN LEE (M'97–SM'05) received the Ph.D. degree in electrical and computer engineering from the University of Texas at Austin, Austin, TX, USA, in 2000.

His current research interests include extreme low-power electronic and photonic device technology using graphene and 2-D materials and the development of electrical characterization methods for silicon devices.